Journal of Power Sources 256 (2014) 288–293

Contents lists available at ScienceDirect

Journal of Power Sources

journal homepage: www.elsevier.com/locate/jpowsour

Short communication

Evaluation of lithium ion cells with titanate negative electrodes and iron phosphate positive electrode for start–stop applications

John S. Wang [a,*], Ping Liu [a], Souren Soukiazian [a], Harshad Tataria [b], Martin Dontigny [c], Abdelbast Guerfi [c], Karim Zaghib [c], Mark W. Verbrugge [d]

[a] Sensors and Materials Lab, HRL Labs, LLC, Malibu, CA, USA
[b] General Motors, Global Electrification, Global Vehicle Engineering, Warren, MI, USA
[c] Institut de Recherche en Électricité d'Hydro-Québec (IREQ), Canada
[d] General Motors, Chemical and Materials Systems Lab, Global R&D, Warren, MI, USA

HIGHLIGHTS

- Investigated the dependence of an LFP/LTO cell energy density on rate and temperature.
- Indicated that improving electrolyte kinetics is the key to enhance low temperature power.
- Pulse cycle tests showed excellent life performance with minimal capacity loss.
- We modeled the circuit parameters of LFP/LTO cell using cyclic voltammetry data.
- Circuit model results indicated the circuit parameters have little SOC dependence.

ARTICLE INFO

Article history:
Received 8 November 2013
Received in revised form
16 January 2014
Accepted 18 January 2014
Available online 24 January 2014

Keywords:
Lithium iron phosphate
$LiFePO_4$
Lithium titanate
$Li_4Ti_5O_{12}$
Start–stop
Battery for vehicle

ABSTRACT

Start–stop systems require the battery to provide high power, endure shallow cycling, and exhibit long cycle life. The LFP/LTO (lithium iron phosphate/lithium titanate) battery is a potential candidate to meet such requirements because, at room temperature, both materials can be operated at high rate and have good stability (calendar and cycle life). In this work, we have investigated the feasibility of using $Li_xFePO_4/Li_{4+3y}Ti_5O_{12}$ ($0 < x < 1$, $0 < y < 1$) lithium ion batteries for start–stop systems. We evaluate both the rate and temperature dependence of LFP/LTO cells subjected to galvanostatic charge/discharge cycling. Excellent rate performance was observed at temperatures above or at ambient. However, at low temperatures, significant resistance is observed, and this must be addressed for the LFP/LTO system to be viable. In addition, we investigate the SOC dependence of equivalent circuit parameters using triangular current and voltage excitation method to facilitate the implementation of circuit-based control algorithms for vehicle applications. Parameter values are nearly constant over the broad voltage-plateau region of the substantially two-phase behavior of both the LFP and LTO materials.

1. Introduction

Implementation of start–stop systems is a pragmatic approach for reducing vehicle fuel consumption. During start–stop operation, the engine automatically shuts down when the vehicle comes to a stop and then quickly restarts when propulsion is desired by the operator.[1] Such start–stop operations of the vehicle can effectively reduce the amount of engine idling time, leading to fuel savings and reducing unwanted emission. Lead-acid batteries are used today for high-volume start–stop vehicle offerings because lead-acid batteries have good low-temperature specific power (kW kg^{-1}) and low initial cost [1]. Frequent high discharge rates can significantly reduce the life of lead acid batteries [2], which motivates the identification of an alternative battery system.

Lithium ion batteries are the leading candidates for automobile applications providing that there are challenges from the cost, and safety perspectives. [3–5] Because of their high specific power and long (cycle and calendar) life, lithium ion batteries are very appealing for power assist vehicular applications. Particularly, Li-ion batteries combining Li_xFePO_4 (LFP, $0 < x < 1$) as the positive

* Corresponding author. 3011 Malibu Canyon Rd., Malibu, CA 90265, USA. Tel.: +1 310 317 5155.
E-mail address: jswang@hrl.com (J.S. Wang).

[1] Typical start–stop systems are designed such that the engine is off when the brake pedal is depressed and the vehicle is stopped. When the operator removes pressure on the brake pedal, the engine starts.

0378-7753/$ – see front matter © 2014 Published by Elsevier B.V.
http://dx.doi.org/10.1016/j.jpowsour.2014.01.079

electrode material and a $Li_{4+3y}Ti_5O_{12}$ (LTO, $0 < y < 1$), as the negative electrode material, can provide significantly improved cycle life, and superior power capability [6]. Both LFP [7–14] and LTO [6,15–17] are known to provide excellent cycle life and rate capability. More importantly, recent developments in nano-engineering of electrode materials significantly improved power capability of lithium ion technology. [13,14,18] Zaghib et al. recently [6] demonstrated that LFP/LTO in an 18650 format cell offers excellent charge/discharge rate capabilities and long life. Hence, the LFP/LTO battery is a promising candidate to meet start–stop requirements.

In this work, we evaluate the feasibility of a commercial grade 18650 LFP/LTO cell using electrochemical methods. First, the rate capabilities of the LFP/LTO cell are investigated using galvanostatic charging and discharging at different temperatures between −30 and 45 °C. The rate performance at high temperatures was excellent while significant resistance rise was observed at low temperatures. Further examination of the temperature dependence of the resistance using the Arrhenius relation suggests the electrolyte resistance limits the cell performance at low temperatures. Further, the cold cranking power is evaluated at −30 °C. We also employ a pulse cycling protocol to examine the long term cycling stability of LFP/LTO. The results are very promising with very minimal capacity and power degradation. Last, we employ a model incorporating electrical circuit elements to correlate the cell behavior. The circuit-element parameters are then regressed from cyclic voltammetry data. Results indicate the circuit parameters (R, R_{ct}, and C) have little SOC dependence. Overall, the LFP/LTO system is a potential candidate for meeting all the requirements for start–stop applications, although a suitable electrolyte composition is needed to improve the low temperature performance.

2. Experimental

2.1. Materials and characterization methods

Commercial grade 18650 cells were prepared that composed of carbon coated $LiFePO_4$ cathode and $Li_4Ti_5O_{12}$ anode. The details of materials synthesis and cell fabrication were published elsewhere. [3] Briefly, $LiFePO_4$ was synthesized through a carbonthermal process using iron and EBN-1010 graphite power as a reducing agent at 1050 °C for 5 min, then used jet-mill and wet-mill in isopropyl alcohol solution process to reduce the particle size to nanoscale. Followed by carbon coating process by mixing the lactose carbon precursor in aqueous solution and heated the final product at 700 °C for 4 h to achieve 2 wt% C $LiFePO_4$. $LiFePO_4$ cathode electrode was made from slurry consisting of 90 wt% of $LiFePO_4$, 6 wt% of carbon black, 2 wt% of CMC and 2 wt% of WSB by using water solvent. $Li_4Ti_5O_{12}$ material was prepared by solid-state reaction of precursor materials TiO_2 and Li_2CO_3 and carbon heated at 850 °C for 18 h. A standard commercial electrolyte of 1 M $LiPF_6$ in EC/DEC was used for the cell fabrication. Capacity characterizations were performed at different temperatures and rates. The tests were conducted using a MACCOR tester (Series 4000). The cells were fully charged to 2.5 V, followed by a voltage hold, and then discharged to 0.5 V. The cell is rated as 1 Ah; therefore, 1 C rate is defined as a constant-current magnitude of 1 A. For Hybrid Pulse Power Characterization (HPPC) tests, taken at every 10% SOC after resting for 1 h, we applied a pulse power sequence which composed of three steps: (1) 5 C charge for 10 s, (2) rest at OCV for 40 s, and (3) 5 C discharge for 10 s. For all the electrochemical testing, a TestEquity environmental chamber (Model 107) was used for the temperature control. Cold cranking tests consist of 2 s discharge and charge pulses at −30 °C and at 30% SOC. Two-second voltage holds at 1.0 V and 2.5 V were applied 3 times with 10 s intervals between each pulse for maximum discharge and charge power determinations, respectively. Long term pulse power cycling stability test was performed using a prescribed profile: (1) discharge for 59 s at 1 C rate, (2) discharge 1 s at 5 C rate, (3) charge 32 s at 2 C rate, and (4) rest for 28 s. The cell was continuously cycled under the prescribed pulse power profile at room temperature. Periodically, the test was interrupted for a C/10 capacity characterization.

The cyclic voltammetry (CV) experiments were carried out using a PAR EG&G 283 potentiostat. Starting at a fully charged state, the cell was discharged at 1 C rate to 80% SOC with a rest of 1hr. Then the voltage was scanned between ±15 mV against the OCV at various rates from 50 to 0.5 mV s^{-1}. The experiments were then repeated for 60, 40, and 20% SOC.

3. Results and discussion

3.1. Electrochemical evaluation

Fig. 1 shows the voltage profile of the LFP/LTO cell subject to galvanostatic charge/discharge at C/2, 2 C, and 5 C rates and at temperatures of −20, 0, 25, and 45 °C. The rate and temperature dependence of the cell capacities are summarized in Fig. 2. The rate capabilities of LFP/LTO cell are excellent at or above room temperature (25 °C). Even at a 5 C rate at 25 °C, the cell maintains 99% of its full capacity. However, as temperature decreases to below 0 °C, we observe an increase in voltage hysteresis between charge and discharge, a clear indication of resistance rise. At −30 °C, capacity retention was about 20–30% of the value at ambient temperatures, even at modest charge/discharge rates (below 2 C rates). The slight increase in capacities in going from 2 to 5 C rates at −20 and 0 °C were a result of improved kinetics due to internal heating at high rates.

We further examined the temperature effects on resistance using HPPC. Fig. 3 shows the discharge and charge resistances plotted as a function of depth of discharge (DOD) at −20, 0, 25, 35, and 45 °C. For the purposes of Fig. 3, discharge and charge resistances were determined using a $\Delta V/\Delta I$ calculation method from pulse power characterizations. The discharge resistance at each specific SOC was calculated from voltage change, ΔV of a constant current discharge pulse divided by the current applied, ΔI at the pulse duration. Similarly, the charge resistance, or regenerative resistance at each SOC was calculated from of a constant current charge pulse divided by the current applied, ΔI at the pulse duration. The details of the calculation procedures can be found elsewhere [19]. It is evident that the resistance increased more significantly at low temperatures (Fig. 3). Arrhenius plots were also constructed for the resistance at 20% DOD in Fig. 4. We observed two distinct linear Arrhenius relation regions and the activation energy were calculated from the slope of the curves from each region. At temperatures below ambient, the activation energy was estimated at 25 kJ mol^{-1} as compared to only 4 kJ mol^{-1} for the region above ambient. In the low temperature region, the activation energy is similar to the value for the electrolyte indicating that the resistance is dominated by the electrolyte. At higher temperatures, very low activation energy suggests the resistance is no longer limited by the electrolyte; solid-phase resistances are often less temperature dependent than those of liquid electrolytes [20], and the higher-temperature results are consistent with the solid-phase resistance dominating at elevated temperatures. Thus, the results are consistent with the assertion that resistance of electrolyte is responsible for the high resistance of the cell at low temperatures.

We have also investigated the cold cranking power capability at −30 °C. The cell was tested at 30% SOC with three 2 s voltage

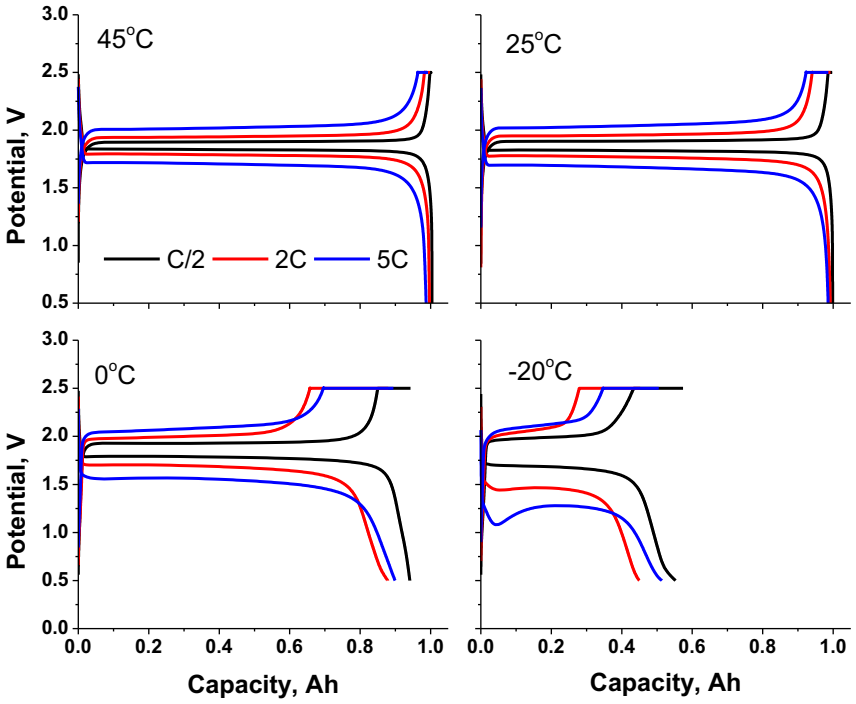

Fig. 1. Charge/discharge behaviors of LFP/LTO cell at different temperatures. 1 Ah 18650 cell is cycled galvanostatically at C/2, 2 C, and 5 C rates: A) 45 °C; B) 25 °C; C) 0 °C; D) −20 °C.

pulses of 1.0 V for discharge power and 2.5 V for charge power. The tests reflect the maximum power available at that specific condition. The results are illustrated in Fig. 5. For comparison, the pulse tests were also performed at 25 °C. The cold (−30 °C) discharge and charge 2 s powers were 3 and 6 W Ah^{-1}, respectively, as compared to the values at 25 °C of 25 and 50 W Ah^{-1} for discharge and charge powers, respectively. Thus, the cold cranking power at −30 °C is about 12% that of room temperature. The cold cranking capability is thus a dominant factor for the battery sizing: improving the low temperature performance of the LFP/LTO cell is critically important in terms of achieving a viable start/stop battery based on this system.

Pulse cycling durability tests were performed to examine the pulse power effects on cell life. We implemented modified testing procedures based on the "SBA S0101 idling-stop life cycling testing protocols." The schematic of the modified testing protocol is shown in the inset of Fig. 6A. To retain the charge/discharge coulomb balance, we design the protocol that the discharge capacity equals to the charge capacity for very cycle. Specifically, we applied 1 C discharge for 59 s combined with 5 C discharge for 1 s, followed by 2 C charge for 32 s then rested the cell for 28 s. This procedure was repeated continuously at 25 °C for 10,000–12,000 cycles at a time. Then the cell was stopped to perform capacity characterizations at C/10 rate. After the capacity characterization, the cell is fully charged to 2.5 V at C/10 rate to get ready for continuing the idling-stop life cycling test. The periodic capacity characterization results were summarized in Fig. 6B. The charge/discharge profiles showed

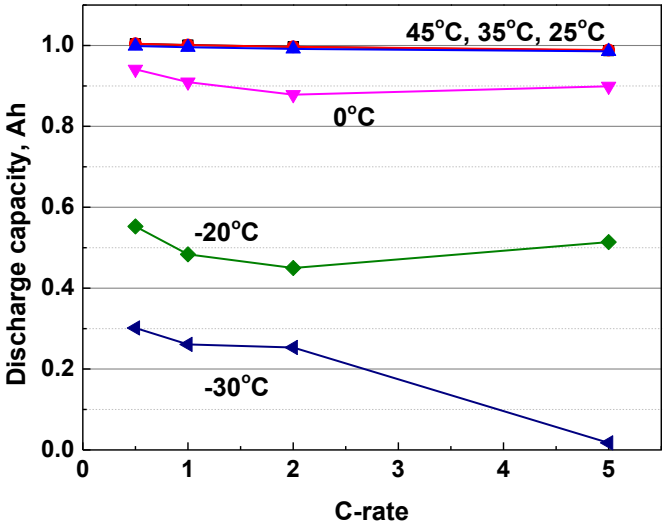

Fig. 2. Discharge capabilities of LFP/LTO cell are plotted as a function of C-rates (C/2, 1 C, 2 C and 5 C) at various temperatures from 45 °C to −30 °C.

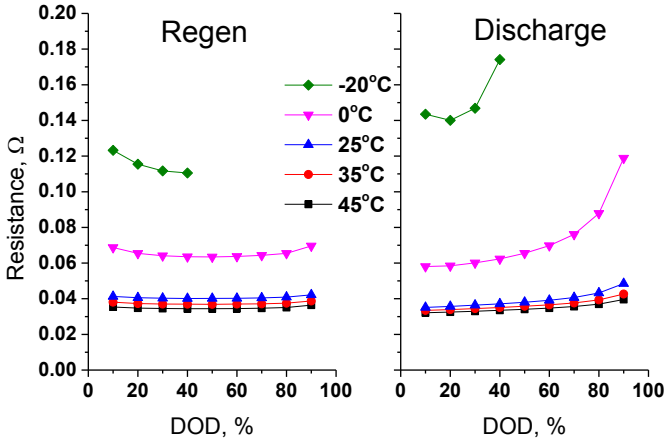

Fig. 3. SOC dependence of discharge/regenerative resistance is plotted at different temperatures between 45 °C and −20 °C.

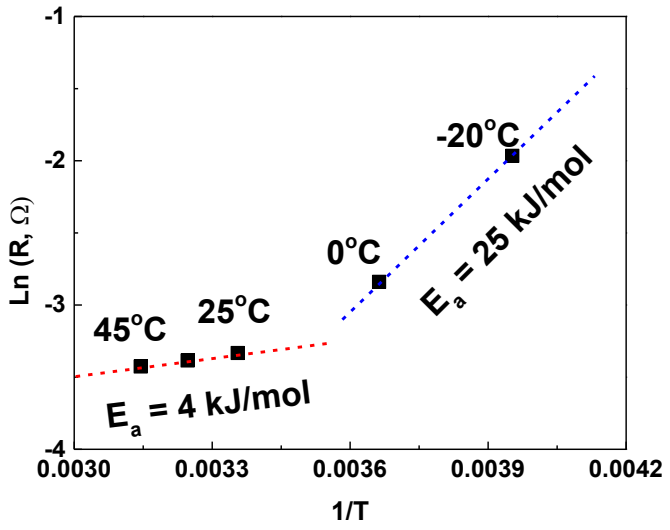

Fig. 4. Log of resistance is plotted as a function of inverse of temperature 1/T at 80% SOC. Results show a summary activation energy calculation using the Arrhenius equation.

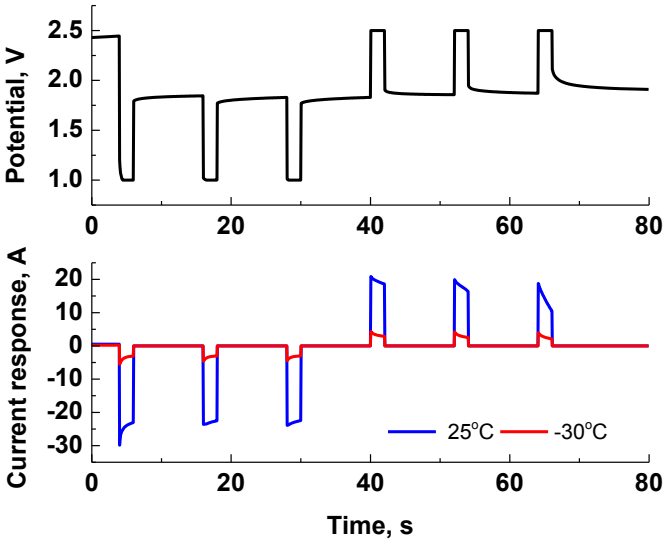

Fig. 5. A comparison of 2 s pulse power evaluation of LFP/LTO cell performed at 25 °C and −30 °C.

no signs of resistance rise after pulse cycling suggesting no observable power fade. In addition, very little capacity losses were observed: 0.2% per 10 k cycles. These results indicated that pulse cycling has minimal impact to the cell capacity and power at room temperature.

3.2. Circuit parameter evaluation of LFP/LTO for vehicle applications

We further performed cyclic voltammetry analysis of the LFP/LTO battery in order to model it using an equivalent circuit, *R–RC*. For vehicle applications, determination of circuit parameters, such as *R*, R_{ct}, and *C* can be employed to assess the state of charge, state of health, and power capabilities of the battery systems [21–26]. The circuit parameters are likely to vary with SOC. Understanding the SOC dependence of parameters facilitates the implementation of circuit-based control algorithms (battery state estimators).

The LFP/LTO cell was characterized using the cyclic voltammetric technique with scan rates ranging from 0.5 to 50 mV s^{-1} at a voltage window of ±15 mV about the open-circuit voltage. We applied a simplified equivalent circuit model comprising of a resistor in series with a parallel resistor–capacitor combination (Fig. 7) to represent the battery. In a previous publication, Verbrugge and Liu, [27] derived analytical solutions based on the described circuit model and successfully demonstrated its application on high-power lithium ion batteries. Briefly, after applying a current balance to the circuit (Fig. 7), the current *I* and voltage *V* can be represented by

$$\frac{dV}{dt} - \frac{1}{R_{ct}C}(V_o - V) = R\frac{dI}{dt} + \frac{1}{C}\left(1 + \frac{R}{R_{ct}}\right)I \quad (1)$$

where *R* is the high frequency resistance, R_{ct} is the interfacial charge-transfer resistance, and *C* is the capacitance. The analytic solution of Eq. (1) is expressed as:

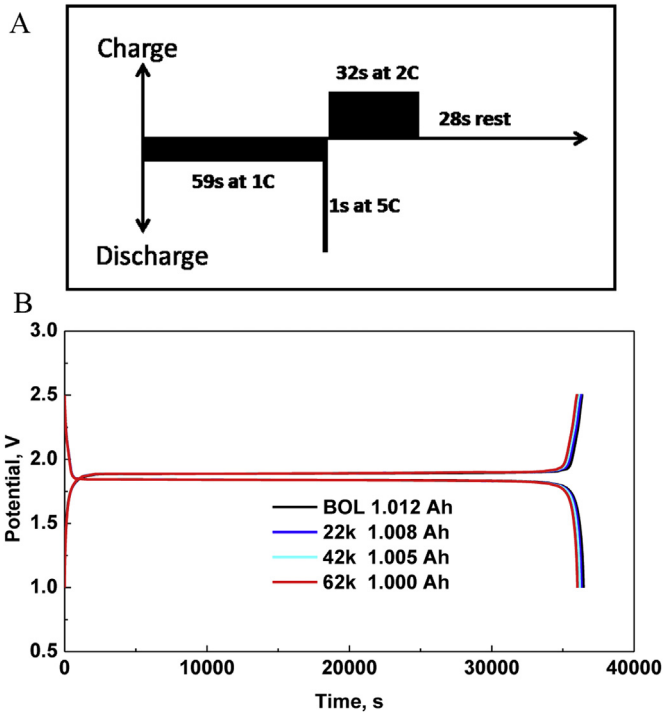

Fig. 6. A) Schematic of prescribed pulse cycle profile; B) C/10 charge/discharge capacity characterizations of LFP/LTO cycled under prescribed pulse cycle profile at 25 °C.

where
$\tau = t/\theta, \tilde{V} = (V - V_o)/(V_{max} - V_0), \tilde{I} = I/\nu C, \alpha = RC/\theta, r = R/R_{ct}, \theta$ is the half − cycle time. The cyclic voltammetric responses obtained from various scan rates can be fitted with the analytic solution (Eq. (2)) to determine the circuit parameters. There are two

$$\tilde{I} = 4\sum_{n=1,3,5,\ldots}^{\infty} \frac{\alpha n\pi \sin[n\pi(\tau + (1/2))] - (\alpha^2 n^2\pi^2 + r + r^2)\cos[n\pi(\tau + (1/2))]}{\alpha n^2\pi^2\left[\alpha^2 n^2\pi^2 + (1+r)^2\right]} \quad (2)$$

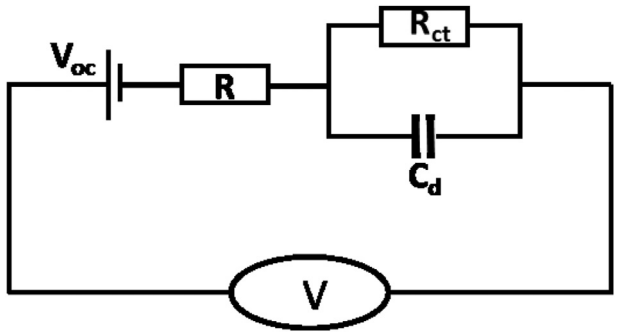

Fig. 7. Schematic of an equivalent circuit model representing the cell behavior.

dimensionless groups that governs the current response to the voltage excitation, $\alpha = RC/\theta$, $r = R/R_{ct}$. As α decreases, the dimensionless currents I/vC increase and reflecting more ohmic behavior in which it leads to increase linearity in the voltammograms and reduced hysteresis. On the other hand, as r decreases, reflecting increase in interfacial resistance, R_{ct}, the I/vC decreases. By varying these two groups of dimensionless terms, one can extract the circuit parameters by fitting the analytical solution (Eq. (2)) with experimental data On Fig. 8 shows the comparison between the analytic simulations of voltammogram and the experimental data at scan rates of 1, 5 and 20 mV s^{-1} and for SOCs at 20, 40, 60 and 80%. The dimensionless, scaled currents correspond to I/vC, where v is the scan rate. The lines represent the analytic stationary-state voltammogram (Eq. (2)) and the markers are experimental collected at each corresponding scan rates. As illustrated in the plots, the analytic results agreed well with the experimental data. The parameters R, R_{ct}, and C extracted from the analysis are plotted

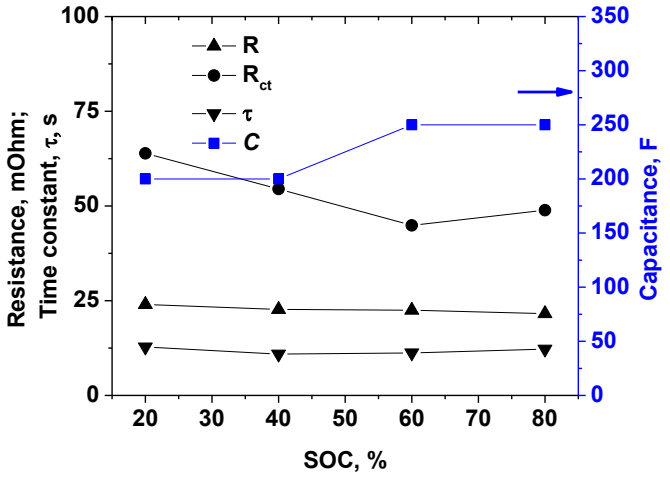

Fig. 9. Summary of equivalent circuit parameters obtained from model fitting of the cyclic voltammetric data for LFP/LTO cell.

in Fig. 9. While the R_{ct} and C show small variations, the high frequency resistance R and the time constant $R_{ct}C$ were fairly constant across the SOC range. The constancy of the parameter values implies that the system chemistry is substantially invariant over the broad constant-voltage plateau that is associated with two-phase behavior in each of the electrodes. The trends in the R, R_{ct}, and C parameters with variation in SOC reveals the insights on how one can build accurate circuit based control algorithms for the battery state estimations. More importantly, the ability of the simple circuit to accurately represent the cyclic response data that equivalent circuit can be implemented to represent this class of titante-based lithium ion batteries for better battery management.

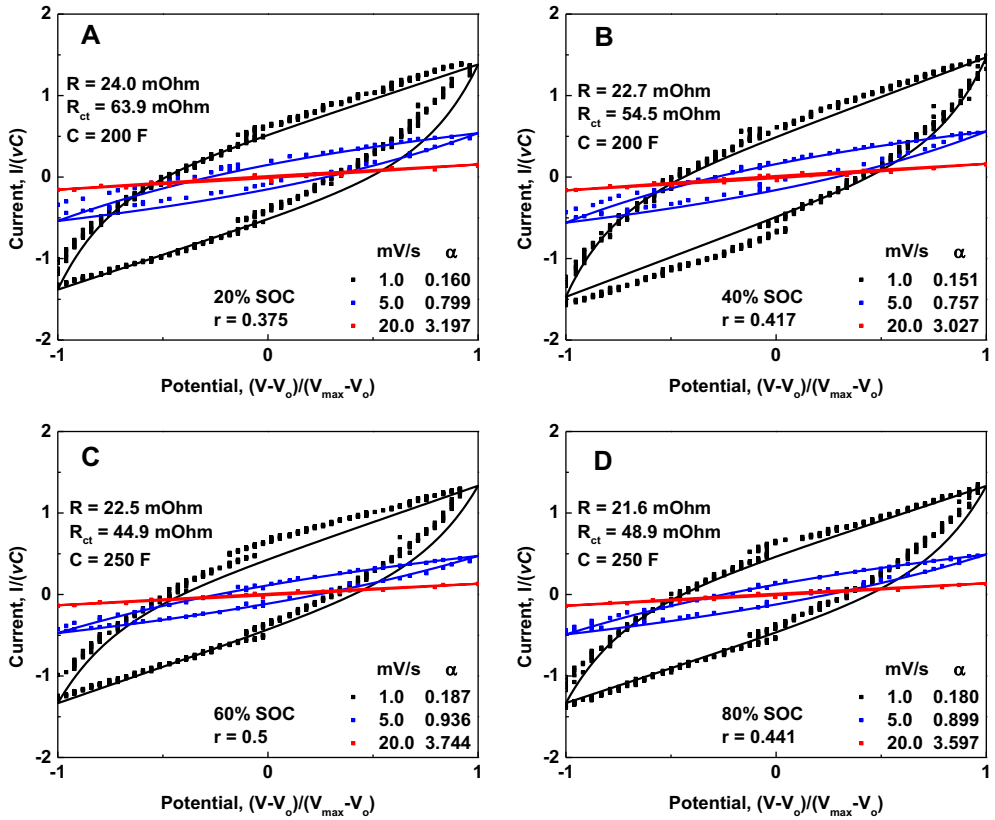

Fig. 8. Experiment-model fitting comparison of the cyclic voltammetric curves for LFP/LTO cell at 20, 40, 60, and 80% SOC.

4. Summary and conclusion

In this paper, we assess the feasibility of LFP/LTO cells for start–stop applications. The dependence of an LFP/LTO cell energy density on rate and temperature was investigated. The cell's rate capabilities are excellent at room temperature or above, but the performance is poor at low temperatures. Examination of the temperature dependence of the resistance revealed that electrode resistance dominates the kinetics at higher temperatures while the electrolyte resistance limits the lower temperature performance. Thus, improving electrolyte conductivity is the key to enhance cell performance at lower temperatures. Pulse cycle durability tests showed minimal coulombic capacity fade at room temperature. At −30 °C, however, both charge and discharge powers decreased by about 12% relative to room temperature. We are developing next generation electrolyte system for enhancing the low temperature power. In addition, we evaluated and quantified the circuit parameter of LFP/LTO cells using cyclic voltammetric method. A very simple equivalent circuit was found to represent well the irreversible losses in the cell. We obtained the circuit parameters of LFP/LTO cell using cyclic voltammetry data combined with an analytical model that represents the battery system. Results indicated the circuit parameters (R, R_{ct}, and C) have little SOC dependence.

References

[1] S. Schaeck, A.O. Stoermer, F. Kaiser, L. Koehler, J. Albers, H. Kabza, J. Power Sources 196 (3) (2011) 1541–1554.
[2] T. Takeuchi, K. Sawai, Y. Tsuboi, M. Shiota, S. Ishimoto, N. Hirai, S. Osumi, J. Power Sources 189 (2) (2009) 1190–1198.
[3] R.J. Brodd, C. Helou, J. Power Sources 231 (2013) 293–300.
[4] B. Canis, Battery Manufacturing for Hybrid and Electric Vehicles: Policy Issues, Congressional Research Service, March 22 2011. R41709(7-5700).
[5] J.B. Goodenough, Y. Kim, J. Power Sources 196 (16) (2011) 6688–6694.
[6] K. Zaghib, M. Dontigny, A. Guerfi, P. Charest, I. Rodrigues, A. Mauger, C.M. Julien, J. Power Sources 196 (8) (2011) 3949–3954.
[7] S.Y. Chung, J.T. Bloking, Y.M. Chiang, Nat. Mater. 1 (2) (2002) 123–128.
[8] B. Kang, G. Ceder, Nature 458 (7235) (2009) 190–193.
[9] A.K. Padhi, K.S. Nanjundaswamy, J.B. Goodenough, J. Electrochem. Soc. 144 (4) (1997) 1188–1194.
[10] N. Ravet, Y. Chouinard, J.F. Magnan, S. Besner, M. Gauthier, M. Armand, J. Power Sources 97–98 (2001) 503–507.
[11] N. Recham, L. Dupont, M. Courty, K. Djellab, D. Larcher, M. Armand, J.M. Tarascon, Chem. Mater. 21 (6) (2009) 1096–1107.
[12] K. Striebel, J. Shim, A. Sierra, H. Yang, X.Y. Song, R. Kostecki, K. McCarthy, J. Power Sources 146 (1–2) (2005) 33–38.
[13] J.W. Fergus, J. Power Sources 195 (4) (2010) 939–954.
[14] A. Manthiram, A. Vadivel Murugan, A. Sarkar, T. Muraliganth, Energy Environ. Sci. 1 (6) (2008) 621–638.
[15] E. Ferg, R.J. Gummow, A. de Kock, M.M. Thackeray, J. Electrochem. Soc. 141 (11) (1994) L147–L150.
[16] T. Ohzuku, A. Ueda, N. Yamamoto, J. Electrochem. Soc. 142 (5) (1995) 1431–1435.
[17] J. Lim, E. Choi, V. Mathew, D. Kim, D. Ahn, J. Gim, S.H. Kang, J. Kim, J. Electrochem. Soc. 158 (3) (2011) A275–A280.
[18] B.L. Ellis, K. Town, L.F. Nazar, Electrochim. Acta 84 (2012) 145–154.
[19] USCAR, USABC Manuals, www.usabc.org.
[20] P. Liu, M. Verbrugge, S. Soukiazian, J. Power Sources 156 (2) (2006) 712–718.
[21] S. Piller, M. Perrin, A. Jossen, J. Power Sources 96 (1) (2001) 113–120.
[22] M. Verbrugge, D. Frisch, B. Koch, J. Electrochem. Soc. 152 (2) (2005) A333–A342.
[23] M. Verbrugge, B. Koch, J. Electrochem. Soc. 153 (1) (2006) A187–A201.
[24] M. Verbrugge, E. Tate, J. Power Sources 126 (1–2) (2004) 236–249.
[25] M.W. Verbrugge, P. Liu, S. Soukiazian, J. Power Sources 141 (2) (2005) 369–385.
[26] S. Wang, M. Verbrugge, J.S. Wang, P. Liu, J. Power Sources 214 (2012) 399–406.
[27] M.W. Verbrugge, P. Liu, J. Power Sources 174 (1) (2007) 2–8.